JOURNAL OF THERMOPHYSICS AND HEAT TRANSFER
Vol. 21, No. 1, January–March 2007

N_2–CH_4–Ar Chemical Kinetic Model for Simulations of Titan Atmospheric Entry

Tahir Gökçen*
ELORET Corporation, NASA Ames Research Center, Moffett Field, California 94035

DOI: 10.2514/1.22095

A detailed chemical kinetic model for N_2–CH_4–Ar mixtures is developed for nonequilibrium simulation of shock layers formed in front of probes entering Titan's atmosphere. The detailed kinetic model uses up-to-date chemical reaction mechanisms and reaction rates, and it is validated against existing shock tube experiments. A reduced kinetic model is also developed through sensitivity analysis of chemical reactions in the detailed model and reproduces the chemical kinetics of major species within the parameter space that may be encountered during Titan atmospheric entry. The reduced model, having fewer species and reactions than the detailed model, is better suited to coupled reacting computational fluid dynamics flowfield calculations.

Downloaded by UNIVERSITY OF QUEENSLAND on August 30, 2021 | http://arc.aiaa.org | DOI: 10.2514/1.22095

Nomenclature

A	=	constant used in evaluating forward rate coefficient
F	=	uncertainty factor for forward rate coefficient
k_f	=	forward rate coefficient
n	=	temperature exponent used in evaluating forward rate coefficient
p	=	pressure
$S_{X,r}$	=	sensitivity coefficient of X with respect to reaction r, defined in the text
$\bar{T}$	=	geometrically averaged temperature, $\sqrt{TT_v}$
T_a	=	temperature constant in forward rate coefficient (activation temperature)
T_r	=	translational-rotational temperature
T_v	=	vibrational-electronic temperature
u	=	x component of velocity

I. Introduction

SHOCK layers formed in front of planetary probes entering the atmosphere of the Saturn moon Titan are expected to be in thermochemical nonequilibrium. Two examples of these probes are the Cassini–Huygens probe scheduled to enter the Titan atmosphere in January 2005, and a Titan probe under consideration by the in-space propulsion program at NASA for future aerocapture missions. Titan's atmosphere is known to be composed primarily of molecular nitrogen, methane, and argon. The relative mole fractions of species are uncertain at this time but believed to be N_2 (80–98%), CH_4 (2–10%), and Ar (0–10%). Methane dissociates behind a strong shock wave at typical hypersonic entry conditions (e.g., speeds of 6–6.5 km/s, nonequilibrium temperatures of 5000–15,000 K, and pressures of 0.01–0.05 atm), and cyano radical (CN) is formed as a result of the nonequilibrium chemistry. Because CN is known to be a strong radiator, the probes are expected to experience significant radiative heating as a result of the nonequilibrium radiation emission from the shock layer. Implications of shock layer nonequilibrium in Titan atmospheric entry were first analyzed by Park [1], and later by others, for example, Nelson et al. [2], Park and Bershader [3], and Park [4]. Several aerothermal analyses carried out relatively recently in [5–11] also indicate that the radiative heating due to CN radiation will be a significant or even the dominant portion of the total heating. The radiative heat flux at the stagnation point was predicted to be as much as 0.5–7.0 times the convective heat flux. There are many reasons for such large variation in the predictions: freestream conditions, the vehicle nose radius (or shock standoff distance), the uncertainty of the CH_4 mole fraction, radiation-flowfield coupling, and the models used for chemistry and radiation. Clearly, a chemical kinetic model plays a pivotal role in the flowfield simulation of a nonequilibrium shock layer and prediction of its radiation.

The chemical kinetic model most commonly used in aerothermal analyses so far was originally proposed by Nelson et al. [2] (Nelson-91 model). However, it is found that this model has several inconsistencies with respect to the current literature: it does not include important species and reactions for methane decomposition and CN formation; and the reaction rates used are significantly different from the current literature values. Therefore, there is a need to update the Nelson-91 model or to develop a new chemical kinetic model for N_2–CH_4–Ar mixtures.

This paper gives a short evaluation of the Nelson-91 model and proposes a new chemical kinetic model consistent with the current literature for simulations of Titan atmospheric entry. For the development of a new chemical kinetic model, the following approach is taken. First, a detailed chemical kinetic model for N_2–CH_4–Ar mixtures is developed using up-to-date chemical reaction mechanisms and reaction rates. Second, the detailed model is validated against four sets of existing shock tube experiments.

Finally, the model is simplified through analysis of the chemical reactions within a parameter space relevant to Titan atmospheric entry. Note that the adjectives "detailed" and "simplified" are used here for kinetic models in the sense that a detailed model is not practical to use in CFD flowfield calculations while a simplified model is.

II. Evaluation of Nelson-91 Chemical Kinetic Model

A summary of chemical reactions and reaction rates used in the Nelson-91 model is given in Table 1. Note that this model was originally described within the framework of Park's two-temperature model (T—translational rotational, T_v—vibrational electronic). Rates of the dissociation reactions are assumed to be governed by an average temperature $\bar{T} = \sqrt{TT_v}$, all exchange reaction rates by T, and all ionization reaction rates by T_v. Nelson et al. do not give details of how the reaction mechanism was obtained and do not give any references for the sources of the reaction rates. However, it appears that the reaction mechanism and some of the reaction rates used are the ones proposed by Park [1].

Presented as Paper 2469 at the 37th AIAA Thermophysics Conference, Portland, Oregon, USA, 28 June–1 July 2004; received 29 December 2005; revision received 13 April 2006; accepted for publication 14 April 2006. Copyright © 2006 by the American Institute of Aeronautics and Astronautics, Inc. The U.S. Government has a royalty-free license to exercise all rights under the copyright claimed herein for Governmental purposes. All other rights are reserved by the copyright owner. Copies of this paper may be made for personal or internal use, on condition that the copier pay the $10.00 per-copy fee to the Copyright Clearance Center, Inc., 222 Rosewood Drive, Danvers, MA 01923; include the code $10.00 in correspondence with the CCC.

*Senior Research Scientist, Member AIAA.

Table 1 Nelson-91 chemical kinetic model and reaction rates

	$k_f = AT^n e^{-T_a/T}$	A, cc/mol/s	n	T_a, K
	Dissociation reactions			
1.	$C_2 + M \rightleftharpoons C + C + M$	9.68×10^{22}	−2.00	71,000
2.	$N_2 + M \rightleftharpoons N + N + M$	3.70×10^{21}	−1.60	113,200
3.	$CH + M \rightleftharpoons C + H + M$	1.13×10^{19}	−1.00	40,913
4.	$CN + M \rightleftharpoons C + N + M$	1.00×10^{23}	−2.00	90,000
5.	$CH_4 + M \rightleftharpoons CH_3 + H + M$	2.25×10^{27}	−1.87	52,900
6.	$CH_3 + M \rightleftharpoons CH_2 + H + M$	2.25×10^{27}	−1.87	54,470
7.	$CH_2 + M \rightleftharpoons CH + H + M$	2.25×10^{27}	−1.87	50,590
8.	$NH + M \rightleftharpoons N + H + M$	1.13×10^{19}	−1.00	41,820
9.	$H_2 + M \rightleftharpoons H + H + M$	1.47×10^{19}	−1.23	51,950
	Exchange reactions			
10.	$C + N_2 \rightleftharpoons CN + N$	1.11×10^{14}	−0.11	23,000
11.	$CN + C \rightleftharpoons C_2 + N$	3.00×10^{14}	0.00	18,120
12.	$C_2 + N_2 \rightleftharpoons CN + CN$	7.10×10^{13}	0.00	5,330
13.	$H + N_2 \rightleftharpoons NH + N$	2.20×10^{14}	0.00	71,370
14.	$H_2 + C = CN + H \rightleftharpoons H_2 + C = CH + H$	1.80×10^{14}	0.00	11,490
15.	$CN^+ + N \rightleftharpoons CN + N^+$	9.80×10^{12}	0.00	40,700
16.	$C^+ + N_2 \rightleftharpoons N_2^+ + C$	1.11×10^{14}	−0.11	50,000
	Ionization reactions			
17.	$N + N \rightleftharpoons N_2^+ + e^-$	1.79×10^{9}	0.77	67,500
18.	$C + N \rightleftharpoons CN^+ + e^-$	1.00×10^{15}	1.50	164,400
19.	$N + e^- \rightleftharpoons N^+ + e^- + e^-$	2.50×10^{34}	−3.82	168,600
20.	$C + e^- \rightleftharpoons C^+ + e^- + e^-$	3.90×10^{33}	−3.78	130,000
21.	$H + e^- \rightleftharpoons H^+ + e^- + e^-$	5.90×10^{37}	−4.00	157,800
22.	$Ar + e^- \rightleftharpoons Ar^+ + e^- + e^-$	2.50×10^{34}	−3.82	181,700

Downloaded by UNIVERSITY OF QUEENSLAND on August 30, 2021 | http://arc.aiaa.org | DOI: 10.2514/1.22095

The Nelson-91 model was evaluated by answering the following two questions: 1) How different are the reaction rates used in the Nelson-91 model from those more recently available in the literature? 2) Does the model have all the important species and reactions to describe the chemistry adequately for CN radiation predictions (if one uses up-to-date reaction rates)?

In answer to the first question, a summary of observations on the reaction rate constants used in the Nelson-91 model is given below. These observations are made for the temperature range of 1000–10,000 K in comparison with the recent literature data to be listed later. The N_2 dissociation rate (heavy-particle impact) is smaller by about a factor of 2 for molecules and an order of magnitude for atoms. The electron-impact dissociation reaction has not been included (or the heavy-particle rate was used). The C_2 dissociation rate is somewhat smaller at higher temperatures (as much as an order of magnitude at 10,000 K). The CH_4, CH_3, and CH_2 dissociation rates are 4–5 orders of magnitude larger.

Note that the low-pressure-limit rates from the literature are used for comparison. The CN dissociation rate is smaller by as much as 1–2 orders of magnitude at lower temperatures, and the activation temperature T_a is different. The NH dissociation rate is larger by as much as an order of magnitude at higher temperatures, and T_a is different. The rate constant of reaction 12 (a CN forming reaction) is much larger, by about 2 orders of magnitude or more, mostly caused by the difference in activation temperatures used. The rate constant of reaction 17 is smaller by about an order of magnitude. The rate constant of reaction 20 is smaller by as much as an order of magnitude, and the rate constant of reaction 21 is larger by as much as 2–3 orders of magnitude. Note that the electron-impact ionization reactions (reactions 19–22) were erroneously listed as heavy-particle reactions in [2]. It should be mentioned here that some of the literature data have large uncertainties themselves since they are extrapolated from the combustion-literature values, usually valid up to 5000 K only.

It is more difficult to evaluate whether the Nelson-91 model has all the important species and reactions to describe the chemistry adequately for CN radiation predictions. However, it is found that the mechanism does not include several radical reactions of CH_3, CH_2, CH, and H in CH_4 decomposition (rates of many of these reactions are of the same order as the CH_4 dissociation rate) and also does not include HCN species and its reactions for CN formation.

It should be noted at this point, without doing any detailed sensitivity analysis of reactions, that the above differences of the Nelson-91 model would translate to significant uncertainties on computed flowfield quantities such as species number densities and temperature (input for CN radiation calculations). It should also be noted that some of the experimental data for reaction rates and reaction mechanisms were not available in the literature when the Nelson-91 was proposed. Therefore, development of a new chemical kinetic model is undertaken.

III. Detailed Chemical Kinetic Model

A detailed chemical kinetic model for N_2–CH_4–Ar mixtures is developed, including the reactions and species potentially present in the parameter space of temperature and pressure relevant to Titan atmospheric entry. The present detailed model includes a total of 74 reactions and 28 chemical species: N_2, CH_4, CH_3, CH_2, CH, C_2, H_2, CN, NH, HCN, N, C, H, Ar, N_2^+, CN^+, N^+, C^+, H^+, Ar^+, e^-, C_2H_6, C_2H_5, C_2H_4, C_2H_3, C_2H_2, C_2H, and C_3.

A summary of chemical reactions and reaction rates used in the detailed model is given in Table 2. As shown in the table, the chemical reaction rates are compiled from various sources. Nitrogen chemistry and reaction rates at high temperatures have been studied by Park in detail [12,13]. Therefore, nitrogen dissociation and ionization reactions and their rates are taken from recent reviews of Park et al. [14–16] Hydrocarbon species reactions and their rates are taken from comprehensive reviews of Baulch et al. [17,18], Tsang [19], Tsang and Herron [20], Tsang and Hampson [21], NIST chemical kinetics database [22], and journal articles [23–31].

A thermodynamic database for the reacting species is an integral part of the chemical kinetic model because reverse reaction rates are computed from the equilibrium constants using the thermodynamic properties. Thermodynamic data and polynomial curve fits for the species of the detailed kinetic model are obtained from the NASA computer program CEA (Chemical Equilibrium with Applications) and its website [32,33]. However, for the hydrocarbon species CH_4, CH_3, CH_2, HCN, C_2H_6, C_2H_5, C_2H_4, C_2H_3, C_2H_2, and C_2H, the thermodynamic data and curve fits are available only up to 6000 K, and most of these curve fits do not produce physical results when extrapolated to higher temperatures (even though hydrocarbon species are expected to be completely dissociated at these temperatures). The range of curve fits is extended linearly by increasing the specific heat from its value at 6000 K to an asymptotic value at 30,000 K. The asymptotic value of the specific heat at 30,000 K for each species is determined by accounting for the

Table 2 Detailed chemical reaction set for N_2–CH_4–Ar mixtures

	$k_f = AT^n e^{-T_a/T}$	A, cc/mol/s	n	T_a, K	Source
		Dissociation reactions			
1.	$N_2 + M \rightleftharpoons N + N + M$	7.00×10^{21}	−1.60	113,200	P(01) [14]
	Enhanced rate for $M = N, C, H$	3.00×10^{22}	−1.60	113,200	P(01) [14]
	Enhanced rate for $M = e^-$	3.00×10^{24}	−1.60	113,200	P(01) [14]
2.	$CH_4 + M \rightleftharpoons CH_3 + H + M$	4.70×10^{47}	−8.20	59,200	B(94) [17]
3.	$CH_3 + M \rightleftharpoons CH_2 + H + M$	1.02×10^{16}	0.00	45,600	B(94) [17]
4.	$CH_3 + M \rightleftharpoons CH + H_2 + M$	5.00×10^{15}	0.00	42,800	DH(92) [23]
5.	$CH_2 + M \rightleftharpoons CH + H + M$	4.00×10^{15}	0.00	41,800	DH(92) [23]
6.	$CH_2 + M \rightleftharpoons C + H_2 + M$	1.30×10^{14}	0.00	29,700	DH(92) [23]
7.	$CH + M \rightleftharpoons C + H + M$	1.90×10^{14}	0.00	33,700	DH(92) [23]
8.	$C_2 + M \rightleftharpoons C + C + M$	1.50×10^{16}	0.00	71,600	KR(97) [27]
9.	$H_2 + M \rightleftharpoons H + H + M$	2.23×10^{14}	0.00	48,350	B(94) [17], B(92) [18]
10.	$CN + M \rightleftharpoons C + N + M$	2.53×10^{14}	0.00	71,000	P(94) [15], T(92) [19]
11.	$NH + M \rightleftharpoons N + H + M$	1.80×10^{14}	0.00	37,600	D(98)-NIST [22]
12.	$HCN + M \rightleftharpoons CN + H + M$	3.57×10^{26}	−2.60	62,845	TH(91) [20]
13.	$C_2H_6 + M \rightleftharpoons CH_3 + CH_3 + M$	6.62×10^{48}	−8.24	47,090	B(94) [17]
14.	$C_2H_5 + M \rightleftharpoons C_2H_4 + H + M$	1.02×10^{18}	0.00	16,800	B(94) [17]
15.	$C_2H_4 + M \rightleftharpoons C_2H_3 + H + M$	2.59×10^{17}	0.00	48,600	B(94) [17]
16.	$C_2H_3 + M \rightleftharpoons C_2H_2 + H + M$	4.16×10^{41}	−7.50	22,900	B(94) [17]
17.	$C_2H_2 + M \rightleftharpoons C_2H + H + M$	6.96×10^{39}	−6.06	67,130	KR(97) [27]
18.	$C_2H + M \rightleftharpoons C_2 + H + M$	1.74×10^{35}	−5.16	57,400	KR(97) [27]
19.	$C_3 + M \rightleftharpoons C_2 + C + M$	4.00×10^{16}	0.00	75,500	KR(97) [27]
		Radical reactions			
20.	$CH_3 + N \rightleftharpoons HCN + H + H$	7.00×10^{13}	0.00	0	D(90) [25]
21.	$CH_3 + H \rightleftharpoons CH_2 + H_2$	6.03×10^{13}	0.00	7,600	B(92) [18]
22.	$CH_3 + CH_4 \rightleftharpoons C_2H_5 + H_2$	1.00×10^{13}	0.00	11,600	TB(79)-NIST [22]
23.	$CH_3 + CH_3 \rightleftharpoons C_2H_4 + H_2$	1.00×10^{14}	0.00	16,100	H(90)-NIST [22]
24.	$CH_3 + CH_3 \rightleftharpoons C_2H_5 + H$	2.40×10^{13}	0.00	6,480	D(95)-NIST [22]
25.	$CH_3 + CH_2 \rightleftharpoons C_2H_2 + H$	4.22×10^{13}	0.00	0	B(94)-NIST [22]
26.	$CH_3 + CH \rightleftharpoons C_2H_3 + H$	1.00×10^{14}	0.00	0	DH(92) [23]
27.	$CH_3 + C \rightleftharpoons C_2H_2 + H$	5.00×10^{13}	0.00	0	DH(92) [23]
28.	$CH_3 + C_2H_6 \rightleftharpoons CH_4 + C_2H_5$	1.50×10^{-7}	6.00	3,040	B(94) [17]
29.	$CH_3 + C_2H_5 \rightleftharpoons CH_4 + C_2H_4$	1.95×10^{13}	−0.50	0	TH(86) [21]
30.	$CH_3 + C_2H_4 \rightleftharpoons CH_4 + C_2H_3$	4.16×10^{12}	0.00	5,600	B(94) [17]
31.	$CH_3 + C_2H_3 \rightleftharpoons CH_4 + C_2H_2$	3.92×10^{11}	0.00	0	TH(86) [21]
32.	$CH_3 + C_2H_2 \rightleftharpoons CH_4 + C_2H$	1.81×10^{11}	0.00	8,700	TH(86) [21]
33.	$CH_2 + N_2 \rightleftharpoons HCN + NH$	4.82×10^{12}	0.00	18,000	S(87)-NIST [22]
34.	$CH_2 + CH_4 \rightleftharpoons CH_3 + CH_3$	4.30×10^{12}	0.00	5,050	Bo(85)-NIST [22]
35.	$CH_2 + N \rightleftharpoons HCN + H$	5.00×10^{13}	0.00	0	D(90) [25]
36.	$CH_2 + N \rightleftharpoons CH + NH$	6.00×10^{11}	0.00	20,400	M(67)-NIST [22]
37.	$CH_2 + C \rightleftharpoons CH + CH$	1.62×10^{12}	0.00	23,600	M(67)-NIST [22]
38.	$CH_2 + H \rightleftharpoons CH + H_2$	6.03×10^{12}	0.00	−900	B(92)-NIST [22]
39.	$CH_2 + CH_2 \rightleftharpoons C_2H_3 + H$	2.00×10^{13}	0.00	0	FJ(84)-NIST [22]
40.	$CH_2 + CH_2 \rightleftharpoons C_2H_2 + H + H$	2.00×10^{14}	0.00	5,530	Ba(95)-NIST [22]
41.	$CH_2 + CH_2 \rightleftharpoons C_2H_2 + H_2$	1.58×10^{15}	0.00	6,010	Ba(95)-NIST [22]
42.	$CH_2 + CH \rightleftharpoons CH + C_2H_2$	4.00×10^{13}	0.00	0	DH(92) [23]
43.	$CH_2 + C \rightleftharpoons C_2H + H$	5.00×10^{13}	0.00	0	DH(92) [23]
44.	$CH_2 + C_2H \rightleftharpoons CH + C_2H_2$	1.81×10^{13}	0.00	0	TH(86) [21]
45.	$CH + N_2 \rightleftharpoons HCN + N$	4.40×10^{12}	0.00	11,060	D(90) [25]
46.	$CH + C \rightleftharpoons C_2 + H$	2.00×10^{14}	0.00	0	DH(92) [23]
47.	$CH + CH_4 \rightleftharpoons C_2H_4 + H$	6.00×10^{13}	0.00	0	DH(92) [23]
48.	$CH + CH \rightleftharpoons C_2H + H$	1.50×10^{14}	0.00	0	DH(92) [23]
49.	$CH + C_2 \rightleftharpoons C_2H + H$	1.00×10^{14}	0.00	0	DH(92) [23]
50.	$CH + C_2H \rightleftharpoons C_2H_2 + C$	1.00×10^{14}	0.00	0	DH(92) [23]
51.	$C_2 + N_2 \rightleftharpoons CN + CN$	1.50×10^{13}	0.00	21,000	S(97) [28]
52.	$C_2 + H_2 \rightleftharpoons C_2H + H$	6.60×10^{13}	0.00	4,030	KR(97) [27]
53.	$C_2 + C_2 \rightleftharpoons C_3 + C$	3.20×10^{14}	0.00	0	KR(97) [27]
54.	$CN + H_2 \rightleftharpoons HCN + H$	2.95×10^{5}	0.00	1,130	W(96) [29]
55.	$CN + C \rightleftharpoons C_2 + N$	5.00×10^{13}	0.00	13,000	P(01) [14]
56.	$N + H_2 \rightleftharpoons NH + H$	1.60×10^{14}	0.00	12,650	DaH(90) [26]
57.	$C + N_2 \rightleftharpoons CN + N$	5.24×10^{13}	0.00	22,600	B(94) [17]
58.	$C + H_2 \rightleftharpoons CH + H$	4.00×10^{14}	0.00	11,700	D(91) [24]
59.	$H + N_2 \rightleftharpoons NH + N$	3.00×10^{12}	0.50	71,400	R(78) [30]
60.	$H + CH_4 \rightleftharpoons CH_3 + H_2$	1.32×10^{4}	3.00	4,045	B(94) [17], B(92) [18]
61.	$H + C_2H_6 \rightleftharpoons C_2H_5 + H_2$	1.45×10^{9}	1.50	3,730	B(94) [17]
62.	$H + C_2H_5 \rightleftharpoons C_2H_4 + H_2$	1.81×10^{12}	0.00	0	TH(86)-NIST [22]
63.	$H + C_2H_4 \rightleftharpoons C_2H_3 + H_2$	5.42×10^{14}	0.00	7,500	B(94) [17]
64.	$H + C_2H_3 \rightleftharpoons C_2H_2 + H_2$	1.20×10^{12}	0.00	0	B(94) [17]
65.	$H + C_2H_2 \rightleftharpoons C_2H + H_2$	6.62×10^{13}	0.00	14,000	B(94) [17]
66.	$C_2H + C \rightleftharpoons C_3 + H$	1.00×10^{14}	0.00	0	DH(92) [23]
		Ionization reactions			
67.	$N + N \rightleftharpoons N_2^+ + e^-$	4.40×10^{7}	1.50	67,500	P(01) [14]
68.	$C + N \rightleftharpoons CN^+ + e^-$	1.00×10^{15}	1.50	164,400	N(91) [2]
69.	$N + e^- \rightleftharpoons N^+ + e^- + e^-$	2.50×10^{34}	−3.82	168,600	P(01) [14], P(93) [16]
70.	$C + e^- \rightleftharpoons C^+ + e^- + e^-$	3.70×10^{31}	−3.00	130,720	P(01) [14]
71.	$H + e^- \rightleftharpoons H^+ + e^- + e^-$	2.20×10^{30}	−2.80	157,800	P(01) [14]
72.	$Ar + e^- \rightleftharpoons Ar^+ + e^- + e^-$	2.50×10^{34}	−3.82	181,700	N(91) [2]
73.	$CN^+ + N \rightleftharpoons CN + N^+$	9.80×10^{12}	0.00	40,700	N(91) [2]
74.	$C^+ + N_2 \rightleftharpoons N_2^+ + C$	1.11×10^{14}	−0.11	50,000	N(91) [2]

Downloaded by UNIVERSITY OF QUEENSLAND on August 30, 2021 | http://arc.aiaa.org | DOI: 10.2514/1.22095

number of atoms, type of molecule, and estimated internal excitations.

IV. Validation of Kinetic Model

Validation of the detailed model against a number of experiments is important to gain confidence in predictions of the model and determine the parameter space in which the model can be used. The detailed model has been validated against the following set of shock tube experiments: the experiments of Dean and Hanson [23], Dean et al. [25], Kruse and Roth [27], and Mick and Roth [31]. These experiments were chosen such that the measurements are sensitive to only a few reactions (or a small subset) of the kinetic model. Therefore, each of these experiments provides validation for certain reactions in the model. Computational simulations of the experiments were performed using the SENKIN and SHOCK programs in the CHEMKIN package. The CHEMKIN code was originally developed at Sandia National Laboratories, and it is currently a commercial code widely used in simulations of combustion problems [34].

A. Shock-Tube Experiments of Dean and Hanson

In the experiments of Dean and Hanson [23], CH and C concentration time histories were measured behind a reflected shock wave in dilute CH_4/Ar mixtures. The CH measurements were made using narrow-linewidth laser absorption, and the C-atom measurements were made using atomic resonance absorption spectroscopy (ARAS). These experiments are important for the model validation because dissociation rates of several hydrocarbon species in the literature were deduced from these measurements and used in the detailed model. It should be mentioned here that very similar CH concentration measurements in CH_4 dissociation were also obtained by Markus and Roth [35], but their data did not include C concentration. Comparisons are made with the more comprehensive data of Dean and Hanson only.

Comparisons of the detailed model simulation results and experimental data for two cases are presented in Fig. 1. It appears that the computed profiles are lagging the measured profiles by 15–20 μs. In the initial 15–20 μs period, the most important reactions for C and CH productions are the reactions 2–7. Dean and Hanson in [23] also presented a kinetic model to fit their experimental data. There are many differences between the present model and their model. The present methyl (CH_3) dissociation rate (reaction 3 in Table 2) is smaller by a factor of 2 than the one used in [23], which is the primary cause of the observed time lag. As will be shown later, the computed C and CH results are very sensitive to this reaction rate. However, this rate in the present model was not changed solely to match the experimental data better. In general, if there is a recommended rate available from a comprehensive review in the literature, for example, Baulch et al. [17], then the recommended rate is used. Also, the present methane dissociation rate (reaction 2 in Table 2) is different from the one used in [23]. In the present model, the low-pressure-limit rate constants are used for all of the pressure-dependent dissociation reactions. This assumption should be reasonably good at these pressures, based on the work of Kiefer and Kumaran [36]. The present CH_4 dissociation rate may also contribute to this discrepancy but to a smaller extent. Despite the observed time lag, the present model predicts experimental peak values of C and CH mole fractions and qualitative shapes of these curves over the entire time history reasonably well. Overall agreement between the computed and measured profiles is considered good, given that the computed mole fractions are sensitive to a number of reaction rates.

Linear sensitivity analysis has been widely used in the combustion literature for analysis of chemical reactions. In the present work, linear sensitivity analysis is also used, as implemented in the SENKIN program of the CHEMKIN package. Sensitivity coefficients are calculated to determine the rate-limiting steps in the production and consumption of certain species. The sensitivity coefficients of computed CH and C mole fractions with respect to the kinetic model reactions are presented in Fig. 2. The following example is helpful for interpretation of sensitivity coefficients: the

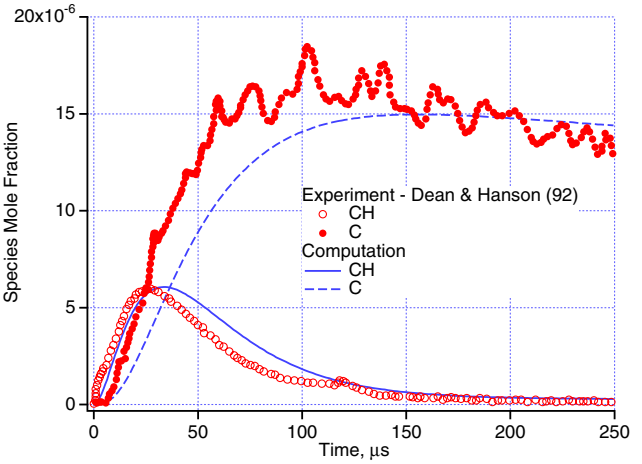

a) p = 0.89 atm, T = 3100 K, 30 ppm CH_4 in Ar.

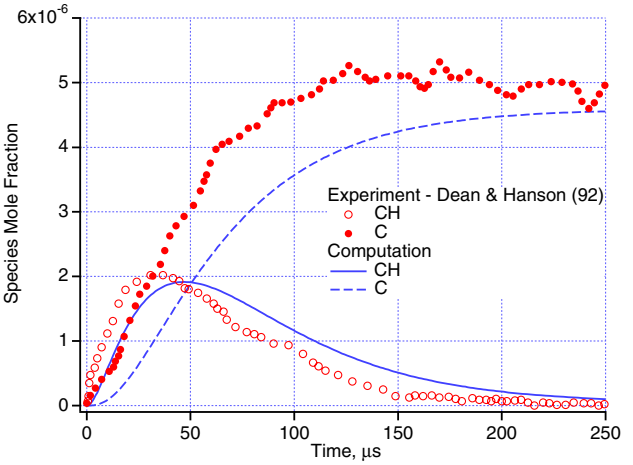

b) p = 0.85 atm, T = 3127 K, 6 ppm CH_4 in Ar.

Fig. 1 Comparison of the detailed model simulation against the shock tube experiments of Dean and Hanson [23] for two cases: time history of CH and C mole fractions.

normalized sensitivity coefficient of parameter X with respect to reaction r (at time level n) is defined as

$$S_{X,r} = \frac{k_r}{X_o} \cdot \frac{\partial X}{\partial k_r}$$

and $S^n_{X,r} = 0.1$ means that if the rate constant for reaction r were doubled, the parameter X would increase by an amount approximately equal to 10% of X_o. The maximum value of X over the time history of the solution is used for the normalization parameter X_o. The computed CH and C results are sensitive to a number of chemical reactions in the detailed model, as shown in Fig. 2. Therefore, these comparisons provide validation for only those reactions affecting CH and C results (a subset of the model).

B. Shock-Tube Experiments of Dean, Hanson, and Bowman

In the experiments of Dean et al. [25], N-atom and CH concentration time histories were measured behind a reflected shock wave in dilute CH_4/Ar and CH_4/N_2–Ar mixtures. The CH measurements were made using narrow-linewidth laser absorption, and the N-atom measurements were made using ARAS. These experiments were chosen because they provide model validation for the reactions of CH and C atoms with N_2. It appears that, almost in parallel, similar work was also carried out by Lindackers et al. [37]. Comparisons are made only with the data from Dean et al.

Comparisons of the detailed model simulation results and experimental data for two cases are presented in Fig. 3. The first case is very similar to the one shown in Fig. 1a (the present experimental

Downloaded by UNIVERSITY OF QUEENSLAND on August 30, 2021 | http://arc.aiaa.org | DOI: 10.2514/1.22095

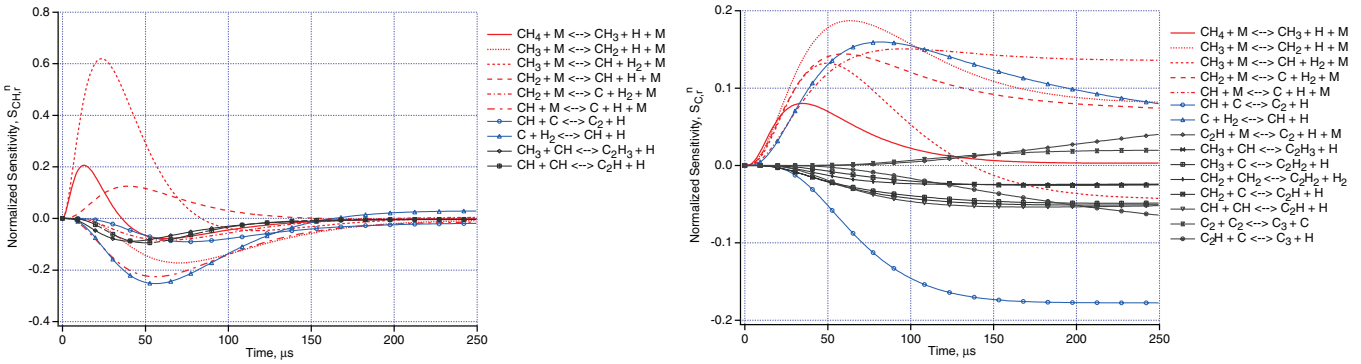

a) CH sensitivity coefficients **b) C sensitivity coefficients**

Fig. 2 Sensitivities of the computed mole fractions to the reaction rates $p = 0.89$ atm, $T = 3100$ K, and 30 ppm CH_4 in Ar.

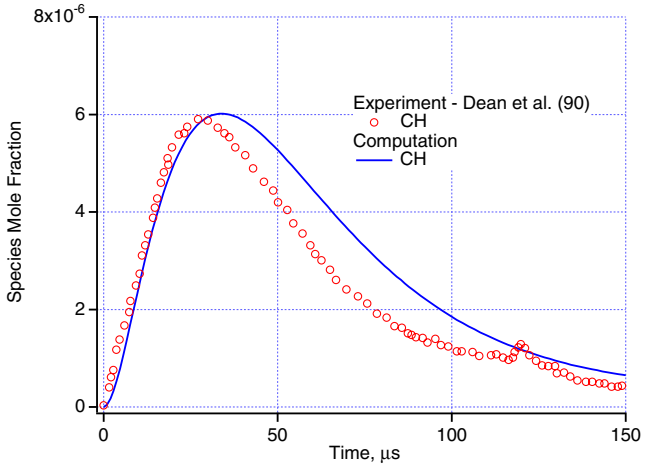

a) $p = 0.89$ atm, $T = 3096$ K, 30 ppm CH_4 in Ar.

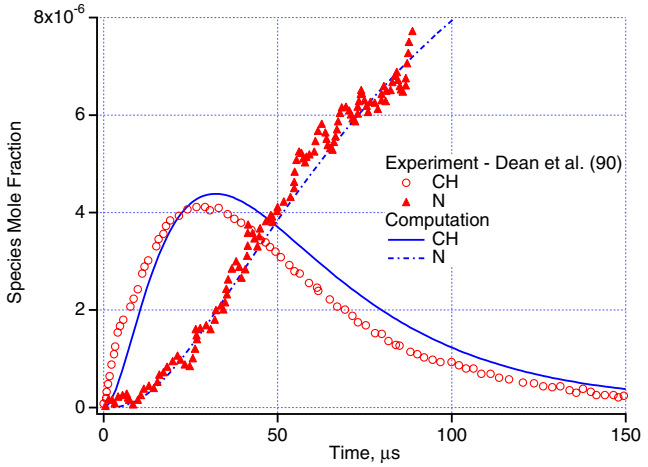

b) $p = 0.88$ atm, $T = 3065$ K, 30 ppm CH_4 and 5% N_2 in Ar.

Fig. 3 Comparison of the detailed model simulation against the shock tube experiments of Dean et al. [25]: time history of CH and N mole fractions.

data were scanned from [25]), for methane pyrolysis in Ar only. The second case includes 5% N_2 and effects of related nitrogen reactions. The measured effect of 5% N_2 on the CH mole fraction is shown in Fig. 3, and it is reproduced by the computations. Agreement between the computed and experimental N-atom profiles is very good within the scatter.

Sensitivity coefficients of the computed N mole fractions with respect to the kinetic model reactions are presented in Fig. 4. The computed results are sensitive to a number of reactions in the detailed model, and a few significant reactions (C-l hydorcarbon reactions having sensitivity coefficients of at least 2%) are marked with an * in the legend of Fig. 4. This case provides validation for those reactions.

C. Shock-Tube Experiments of Kruse and Roth

In the experiments of Kruse and Roth [27], C_2 concentration time histories were measured behind a reflected shock wave using ring dye laser absorption spectroscopy in dilute C_2H_2/Ar mixtures. C and C_3 were also measured using ARAS and emission spectroscopy, respectively. Although the experiments covered the temperature range of 2580–4650 K, as a validation case, C_2 concentration time history at a relatively high temperature of 4450 K was chosen. These experiments provide validation for the rates of several C_2 and C_2H reactions.

Comparison of the computed and experimental C_2 number densities is presented in Fig. 5. Although the detailed model underpredicts the amount of C_2 formed in the first 200 μs, overall agreement between the computed and experimental profiles is reasonably good. Kruse and Roth using a different kinetic mechanism for C_2H_2 pyrolysis obtained a better fit for their measurements but only after modifying C_2 thermodynamic data. They also suggested that JANAF thermodynamic data for either C, C_2, or C_3 be modified in order to explain their experimental data. In the present work, the thermodynamic database was not modified. For this case, the computed C_2 mole fractions are sensitive to only a few reactions, but C_2 sensitivity coefficients to these reactions are relatively large, especially in the first 40 μs. The sensitivity coefficients of computed C_2 mole fractions with respect to the kinetic model reactions are presented in Fig. 6. Since the reaction rates of all the reactions in Fig. 6 are obtained from Kruse and Roth, the differences observed in Fig. 5 are most likely due to the differences in the thermodynamic database used in both models.

D. Shock-Tube Experiments of Mick and Roth

In the experiments of Mick and Roth [31], N concentration time histories were measured behind a reflected shock wave using ARAS in dilute C_2N_2/Ar mixtures. These experiments were chosen because they provide validation for the CN dissociation rate used in the model. For simulation of the experiments, the reaction $C_2N_2 + M \rightleftharpoons CN + CN + M$ is added to the kinetic model, with the forward rate constant $k_f = 1.07 \times 10^{34} T^{-4.32} e^{-65{,}420/T}$ cm^3/mol $\cdot$ s obtained from [31].

Comparisons of the detailed model simulation results and experimental data for one case are presented in Fig. 7. C_2N_2 decomposes rapidly and provides a well-characterized CN source, and N atoms are formed from CN dissociation. The computations predict the experimental N number density over the time history very well. Although sensitivity coefficients are not shown here, the computed N number density is primarily sensitive to the CN dissociation rate (reaction 10) and the reaction 57 in Table 2.

For all validation cases, comparisons between the measurements and detailed model predictions are reasonably good. However, it should be cautioned that all these experiments are at relatively low

Downloaded by UNIVERSITY OF QUEENSLAND on August 30, 2021 | http://arc.aiaa.org | DOI: 10.2514/1.22095

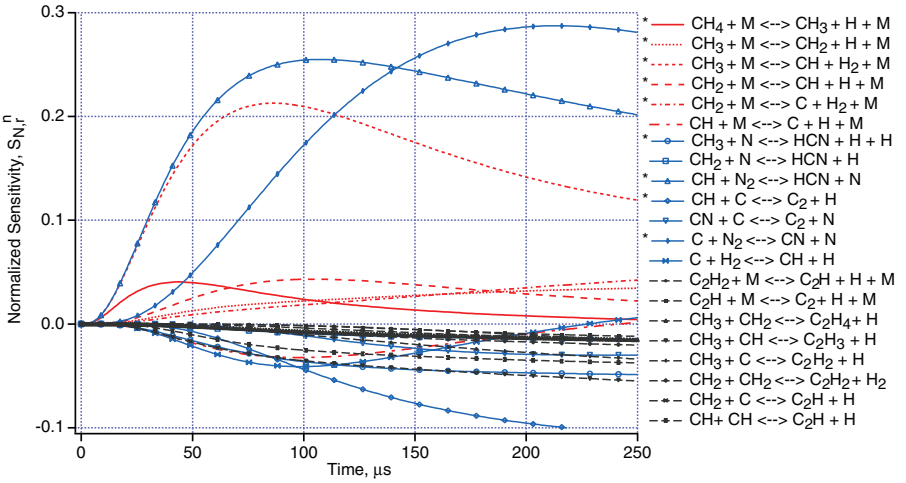

Fig. 4 Sensitivity coefficients of the computed N mole fractions to the reaction rates, $p = 0.88$ atm, $T = 3065$ K, 30 ppm CH_4, and 5% N_2 in Ar.

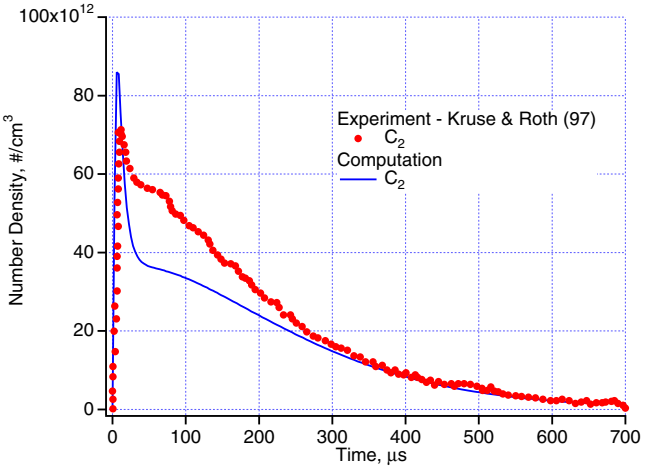

Fig. 5 Comparison of the detailed model simulation against the shock tube experiments of Kruse and Roth [27]: time history of C_2 number density at $p = 1.82$ bar, $T = 4450$ K, and 50 ppm C_2H_2 in Ar.

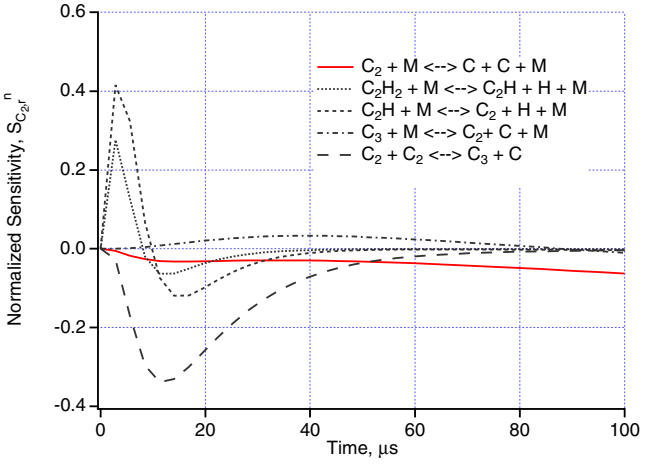

Fig. 6 Sensitivity coefficients of the computed C_2 mole fractions to the reaction rates for the first 100 μs, $p = 1.82$ bar, $T = 4450$ K, and 50 ppm C_2H_2 in Ar.

temperatures ($T \leq 5000$ K). For Titan atmospheric entry, the model will be extrapolated to much higher shock layer temperatures. Nevertheless, these validation cases provide a strong foundation for the N_2–CH_4–Ar model development.

After this model was presented in an AIAA paper [38], shock tube experiments were conducted at the NASA Ames EAST facility at conditions representative of the peak heating point of a Titan aerocapture trajectory. Analysis of these experiments has not been completed yet but the experiments should provide important validation data for the developed model [39].

V. Sensitivity Analysis and Simplification: Reduced Model

Even though the detailed model can easily be used for one-dimensional CFD analysis of shock tube flows, it is too complex and costly to implement in a 2-D or 3-D CFD flowfield code for aerothermal analysis. For this purpose, the detailed model is reduced through analysis of the chemical reactions.

For simplification of chemical species and reactions in the model, the following approach is taken. A parameter space of temperature and pressure relevant to Titan entry is estimated. Through analysis of chemical reactions within this parameter space, certain reactions and species are eliminated from the detailed model. In general, all the species that do not exist within the parameter space in any significant amounts ($\leq 0.2\%$ per mol at maximum) are eliminated. However, the following considerations are also taken into account: the species known to be strong radiators (e.g., CN, N_2^+, NH, CH, C_2, etc.) and their reactions are included whether these species exist in any

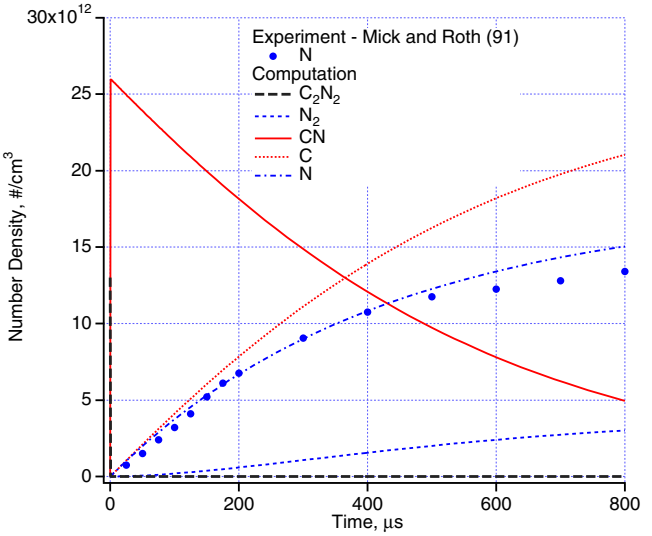

Fig. 7 Comparison of the detailed model simulation against the shock tube experiments of Mick and Roth [29]: time history of N number density at $p = 1.9$ bar, $T = 5290$ K, and 5 ppm C_2H_2 in Ar.

Downloaded by UNIVERSITY OF QUEENSLAND on August 30, 2021 | http://arc.aiaa.org | DOI: 10.2514/1.22095

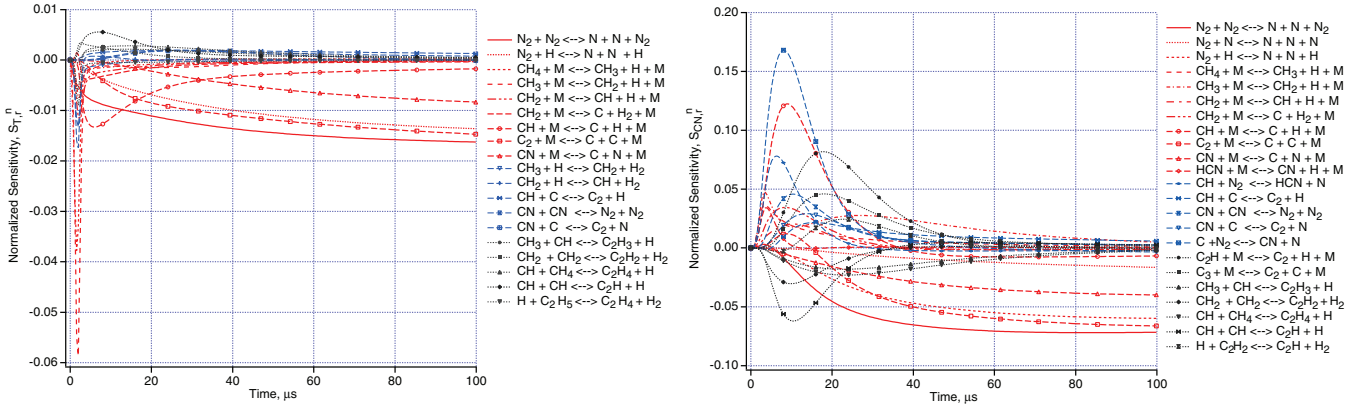

a) T sensitivity coefficients **b) CN sensitivity coefficients**

Fig. 8 Sensitivity coefficients of temperature and CN mole fractions to the reaction rates at constant pressure, $p = 0.05$ atm. Initial conditions: $T_i = 10,000$ K, and 5% CH_4 in N_2.

significant amounts or not; and certain species (e.g., CH_3, CH_2, HCN, CN^+) which do not exist in any significant amounts but do provide important reaction paths through their reactions for methane decomposition and CN formation are also included. Sensitivity analysis is an important tool to eliminate unimportant species and reactions. In addition, sensitivity analysis of flowfield variables that influence CN radiation computations is performed to reduce the detailed model within the parameter space of interest.

For typical Titan entry trajectories (e.g., see Nelson et al. [2], Takashima et al. [8], Olejniczak et al. [9]), when shock layers in front of the probes at anticipated entry velocities and altitudes are considered, it is estimated that pressures at the stagnation point behind the shock wave range from 0.01 to 0.05 atm, and the shock layer temperatures range from 5000 to 15,000 K. Also, for a typical shock standoff distance of 10 cm, at various entry speeds in the range of 3.0–6.5 km/s, examining chemistry of particles behind the shock wave over a time period of 100 μs is estimated to be sufficient for predicting radiative heating to the stagnation point.

Because our primary interest is to simulate nonequilibrium radiation emission from the shock layer due to CN, accurate

Table 3 Reduced chemical reaction set for N_2–CH_4–Ar mixtures

	$k_f = AT^n e^{-T_a/T}$	A, cc/mol/s	n	T_a, K	Source/uncert. est.
		Dissociation reactions			
1.	$N_2 + M \rightleftharpoons N + N + M$	7.00×10^{21}	−1.60	113,200	P(01) [14]/$F = 3.0$
	Enhanced rate for $M =$ N, C, H	3.00×10^{22}	−1.60	113,200	P(01) [14]/$F = 3.0$–5.0
	Enhanced rate for $M = e^-$	3.00×10^{24}	−1.60	113,200	P(01) [14]/$F = 5.0$
2.	$CH_4 + M \rightleftharpoons CH_3 + H + M$	4.70×10^{47}	−8.20	59,200	B(94) [17]/$F = 2.0$
3.	$CH_3 + M \rightleftharpoons CH_2 + H + M$	1.02×10^{16}	0.00	45,600	B(94) [17]/$F = 1.26$–3.2
4.	$CH_3 + M \rightleftharpoons CH + H_2 + M$	5.00×10^{15}	0.00	42,800	DH(92) [23]/$F = 1.26$–2.0
5.	$CH_2 + M \rightleftharpoons CH + H + M$	4.00×10^{15}	0.00	41,800	DH(92) [23]/$F = 1.26$–2.0
6.	$CH_2 + M \rightleftharpoons C + H_2 + M$	1.30×10^{14}	0.00	29,700	DH(92) [23]/$F = 1.26$–2.0
7.	$CH + M \rightleftharpoons C + H + M$	1.90×10^{14}	0.00	33,700	DH(92) [23]/$F = 1.26$–2.0
8.	$C_2 + M \rightleftharpoons C + C + M$	1.50×10^{16}	0.00	71,600	KR(97) [27]/$F = 1.26$–2.0
9.	$H_2 + M \rightleftharpoons H + H + M$	2.23×10^{14}	0.00	48,350	B(94) [17], B(92) [18]/$F = 1.26$–2.0
10.	$CN + M \rightleftharpoons C + N + M$	2.53×10^{14}	0.00	71,000	P(94) [15], T(92) [19]/$F = 1.5$–2.0
11.	$NH + M \rightleftharpoons N + H + M$	1.80×10^{14}	0.00	37,600	D(98)-NIST [22]/$F = 1.26$–2.0
12.	$HCN + M \rightleftharpoons CN + H + M$	3.57×10^{26}	−2.60	62,845	TH(91) [20]/$F = 1.5$–2.0
		Radical reactions			
13.	$CH_3 + N \rightleftharpoons HCN + H + H$	7.00×10^{13}	0.00	0	D(90) [25]/$F = 10.0$
14.	$CH_3 + H \rightleftharpoons CH_2 + H_2$	6.03×10^{13}	0.00	7,600	B(92) [18]/$F = 10.0$
15.	$CH_2 + N_2 \rightleftharpoons HCN + NH$	4.82×10^{12}	0.00	18,000	S(87)-NIST [22]/$F = 10.0$
16.	$CH_2 + N \rightleftharpoons HCN + H$	5.00×10^{13}	0.00	0	D(90) [25]/$F = 10.0$
17.	$CH_2 + H \rightleftharpoons CH + H_2$	6.03×10^{12}	0.00	−900	B(92)-NIST [22]/$F = 5.0$–10.0
18.	$CH + N_2 \rightleftharpoons HCN + N$	4.40×10^{12}	0.00	11,060	D(90) [25]/$F = 1.5$–3.2
19.	$CH + C \rightleftharpoons C_2 + H$	2.00×10^{14}	0.00	0	DH(92) [23]/$F = 10.0$
20.	$C_2 + N_2 \rightleftharpoons CN + CN$	1.50×10^{13}	0.00	21,000	S(97) [28]/$F = 1.26$–2.0
21.	$CN + H_2 \rightleftharpoons HCN + H$	2.95×10^{5}	0.00	1,130	W(96) [29]/$F = 3.2$–5.0
22.	$CN + C \rightleftharpoons C_2 + N$	5.00×10^{13}	0.00	13,000	P(01) [14]/$F = 2.0$–5.0
23.	$N + H_2 \rightleftharpoons NH + H$	1.60×10^{14}	0.00	12,650	DaH(90) [26]/$F = 1.26$–2.0
24.	$C + N_2 \rightleftharpoons CN + N$	5.24×10^{13}	0.00	22,600	B(94) [17]/$F = 1.6$–2.0
25.	$C + H_2 \rightleftharpoons CH + H$	4.00×10^{14}	0.00	11,700	D(91)/$F = 1.6$–2.0
26.	$H + N_2 \rightleftharpoons NH + N$	3.00×10^{12}	0.50	71,400	R(78) [30]/$F = 2.0$–3.2
27.	$H + CH_4 \rightleftharpoons CH_3 + H_2$	1.32×10^{4}	3.00	4,045	B(94) [17], B(92) [18]/$F = 1.6$–2.0
		Ionization reactions			
28.	$N + N \rightleftharpoons N_2^+ + e^-$	4.40×10^{7}	1.50	67,500	P(01) [14]/$F = 10.0$
29.	$C + N \rightleftharpoons CN^+ + e^-$	1.00×10^{15}	1.50	164,400	N(91) [2]/$F \geq 10.0$
30.	$N + e^- \rightleftharpoons N^+ + e^- + e^-$	2.50×10^{34}	−3.82	168,600	P(01) [14], P(93) [16]/$F = 10.0$
31.	$C + e^- \rightleftharpoons C^+ + e^- + e^-$	3.70×10^{31}	−3.00	130,720	P(01) [14]/$F = 10.0$
32.	$H + e^- \rightleftharpoons H^+ + e^- + e^-$	2.20×10^{30}	−2.80	157,800	P(01) [14]/$F \geq 10.0$
33.	$Ar + e^- \rightleftharpoons Ar^+ + e^- + e^-$	2.50×10^{34}	−3.82	181,700	N(91) [2]/$F \geq 10.0$
34.	$CN^+ + N \rightleftharpoons CN + N^+$	9.80×10^{12}	0.00	40,700	N(91) [2]/$F \geq 10.0$
35.	$C^+ + N_2 \rightleftharpoons N_2^+ + C$	1.11×10^{14}	−0.11	50,000	N(91) [2]/$F \geq 10.0$

Downloaded by UNIVERSITY OF QUEENSLAND on August 30, 2021 | http://arc.aiaa.org | DOI: 10.2514/1.22095

simulation of the following variables is considered important for Titan entry: temperature, and the number densities of N, CN, H, and e^-. It is believed that sensitivities of these four species number densities and temperature to chemical reactions would provide sufficient redundancy to allow elimination of unimportant reactions for CN radiation emission calculations. Sensitivity coefficients of these variables are computed at constant pressures of 0.01, 0.025, 0.05, 0.1, and 0.5 atm, and initial temperatures of 5000, 8000, 10,000, and 15,000 K over a time period of 100 μs. The pressure range up to 0.5 atm is considered because some of the existing shock tube experiments for Titan entry were obtained at higher pressures [3–5,7]. Note that the temperature and pressure ranges and the time period are chosen for shock layer simulations of Titan atmospheric entry only. From the sensitivity calculations performed, all the reactions not affecting either temperature or the number densities of N, CN, H, and e^- within the parameter space are eliminated.

For one representative case, computed sensitivity coefficients of temperature and CN mole fractions with respect to the kinetic model reactions are shown in Fig. 8. These calculations are carried out at constant pressure of 0.05 atm, and initial conditions are 5% CH_4 in N_2 at a temperature of 10,000 K. As expected, the computed temperature is mostly sensitive to the dissociation reactions of molecules and a few radical reactions. The CN sensitivies shown in Fig. 8b indicate that CN mole fractions are sensitive to a number of radical reactions (in addition to the dissociation reactions). It is interesting to note that some of the C-2 hydrocarbon chemistry reactions (i.e., reactions of the species that have two carbon atoms) are also affecting the CN mole fractions, especially in the first 20 μs. Obviously, these sensitivities strongly depend on the prescribed pressure and initial conditions. At higher pressures, the methane dissociation is completed much faster, and its effect on CN formation is limited to a shorter time period. At lower pressures, the methane dissociation proceeds at a slower rate and its effect on CN formation is spread over a longer time period.

From the analysis of chemical reactions, it is found that for shock layer analysis of Titan entry, the detailed model can be reduced to a model consisting of 21 species (N_2, CH_4, CH_3, CH_2, CH, C_2, H_2, CN, NH, HCN, N, C, H, Ar, N_2^+, CN^+, N^+, C^+, H^+, Ar^+, and e^-) and 35 reactions. In other words, the reduced chemical reaction set would be sufficient for flowfield simulations of temperature and number densities of N, CN, H, and e^-. A summary of chemical reactions and reaction rates used in the reduced model is given in Table 3. Further simplification of the model is possible by eliminating some of the radical–radical reactions (e.g., reactions 13, 15, 16, 17, 35), but they are retained here because of their uncertainties.

In Table 3, the uncertainty factors (F) for each reaction rate in the reduced model (as well as the source) are also listed. Following the notation of Baulch et al. [17], F is defined such that the range of values of k_f is bounded by multiplication and division of k_f by a factor F. It is difficult to put uncertainty factors on these reaction rates

Downloaded by UNIVERSITY OF QUEENSLAND on August 30, 2021 | http://arc.aiaa.org | DOI: 10.2514/1.22095

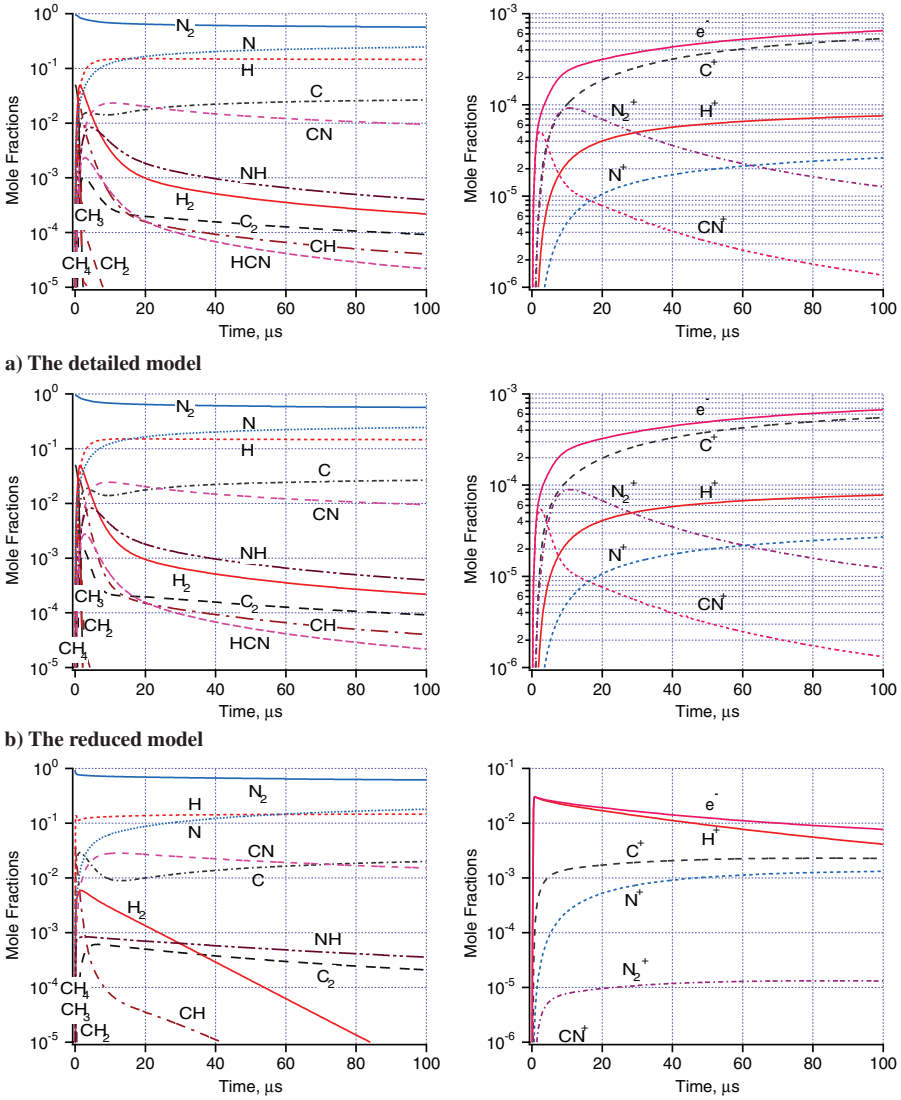

Fig. 9 The time histories of computed mole fractions using different kinetic models: shock tube flow, $p_1 = 0.1$ torr, $T_1 = 300$ K, $u_1 = 6.3$ km/s, and 5% CH_4 in N_2. Neutral and charged species are shown separately.

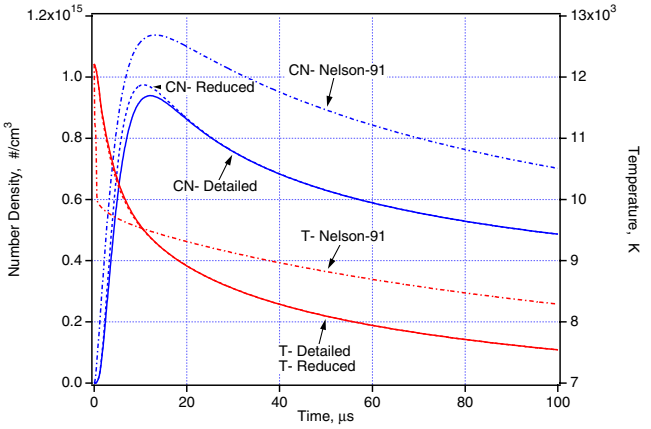

Fig. 10 Comparisons of the computed CN number densities and temperatures using different models: shock tube flow, $p_1 = 0.1$ torr, $T_1 = 300$ K, $u_1 = 6.3$ km/s, and 5% CH_4 in N_2.

because shock layer temperatures for Titan entry are much higher than the temperature range over which these rates are reviewed and measured. Therefore, these F factors should be considered a lower limit on the uncertainty. Some of these uncertainty factors are obtained from the review articles cited, and some are purely based on subjective judgement of the author (based on literature surveys and the uncertainties on similar reaction rates). Even though it is subjective, it is still useful to have some estimate of the reaction rate uncertainties. These uncertainty factors are used in a paper by Bose et al. [40] for uncertainty analysis of the thermochemical modeling for Titan atmosheric entry.

VI. Sample Case: Shock-Tube Flow at $u_1 = 6.3$ km/s

A sample case of shock tube flow, duplicating typical shock layer conditions in Titan atmospheric entry, is chosen to present simulations using the different kinetic models. All simulations use a one-temperature model. Figure 9 shows the computed species mole fractions as functions of time using the detailed, reduced, and Nelson-91 models.

As shown in Fig. 9, the detailed model predicts that at these conditions methane decomposition is completed within 10 μs. Afterwards, the major species remaining are N_2, N, H, C, CN, NH, H_2, C_2, CH, and HCN. Although this case does not involve significant ionization, CN^+ associative ionization reaction provides an initial ionization path. C^+, N_2^+, and H^+ represent the most significant ionized species.

The reduced model results in comparison with the detailed model results show minor differences in terms of major species, which is not coincidental of course because the reduced model was developed based upon those criteria. The main differences are within the first 10–20 μs, and even in that range, the maximum differences between the detailed and reduced model predictions of N_2, N, CN, an H mole fractions are less than 0.006, 0.001, 0.0025, and 0.003, respectively.

In Fig. 9c, the Nelson-91 model results for species mole fractions are presented. In comparison with the detailed model results, there are significant differences (as expected from the evaluation of the Nelson-91 model). The Nelson-91 model predicts that at these conditions methane decomposition is almost instantaneous, due to the much larger methane dissociation rates used. The major species remaining afterwards are N_2, N, H, C, CN, NH, C_2, H_2, and CH. In comparison with the detailed model values, computed CN levels are higher and N levels are lower. The Nelson-91 model also predicts much higher ionization levels than the detailed model. Electron-impact ionization of H is the dominant ionization reaction (reaction 21 in Table 1), and H^+, C^+, and N^+ represent the most significant ionized species. Note that if these calculations were carried out using a two-temperature model, the computed ionization levels would be smaller.

Finally, comparisons of CN number densities and temperatures using different models are presented in Fig. 10. CN number density and temperature are the most important flowfield parameters affecting computations of shock layer radiation due to CN. The present model predicts lower CN number densities and lower temperatures behind the shock in comparison with the Nelson-91 model. Although computation of radiative heating to Titan probes is outside the scope of this paper, it is expected that the radiative heating computed with the present model would be much smaller than what the Nelson-91 model would suggest.

VII. Concluding Remarks

A detailed chemical kinetic model for N_2–CH_4–Ar mixtures is developed for nonequilibrium flowfield simulation of shock layers formed in front of probes entering Titan's atmosphere. The detailed kinetic model uses up-to-date chemical reaction mechanisms and reaction rates consistent with the literature, and it is validated against existing shock tube experiments. For all the validation cases presented, comparisons between the measurements and detailed model predictions are reasonably good, and these cases provide a strong foundation for the present kinetic model. It should be cautioned that all these experiments are at relatively low temperatures ($T \leq 5000$ K), and that for Titan atmospheric entry applications, the reaction rates used in the model will be extrapolated to much higher shock layer temperatures. Further validation studies are needed to reduce uncertainties and increase the confidence level of predictions. The shock tube experiment program recently conducted at the NASA Ames EAST facility to measure the radiation from N_2–CH_4 shock waves at velocities relevant to Titan atmospheric entry (6–6.5 km/s) should provide additional validation data for the detailed model.

A reduced kinetic model having fewer species and reactions than the detailed model is also developed for coupled reacting CFD flowfield calculations. There are important differences between the present kinetic model and the Nelson-91 model in terms of species and reaction mechanisms for methane decomposition and CN formation and the reaction rates used. As mentioned, a chemical kinetic model is only one of the building blocks used in shock layer radiation analysis. A complete radiative heating analysis of Titan probes is outside the scope of the present paper. However, the models developed provide a suitable foundation for such analysis.

Acknowledgments

This work was funded by the In-Space Propulsion program under task agreement M-ISP-03-18 to NASA Ames Research Center. The support from NASA Ames Space Technology Division through contract NAS2-99092 to the ELORET Corporation is gratefully acknowledged.

References

[1] Park, C., "Radiation Enhancement by Nonequilibrium During Flight Through The Titan Atmosphere," AIAA Paper 82-0878, June 1982.

[2] Nelson, H. F., Park, C., and Whiting, E. E., "Titan Atmospheric Composition by Hypervelocity Shock-Layer Analysis," *Journal of Thermophysics and Heat Transfer*, Vol. 5, No. 2, 1991, pp. 157–165; also AIAA Paper 89-1770, June 1989.

[3] Park, C. S., and Bershader, D., "Determination of the Radiative Emission of Hypersonic Flow Simulating the Cassini-Titan Atmospheric Entry Probe Environment," AIAA Paper 90-1558, June 1990.

[4] Park, C. S., "Studies of Radiative Emission from the Simulated Shock Layer of the Huygens Probe," Ph.D. Dissertation, Stanford University, Stanford, CA, 1991.

[5] Bailion, M., and Taquin, G., "Radiative Heat Flux: Theoretical and Experimental Predictions for Titan Entry Probe," Capsule Aeorothermodynamics, AGARD Report R-808, May 1997.

[6] Bailion, M., Pallegoix, J. F., and Soler, J., "Huygens Probe Aerothermodynamics," AIAA Paper 97-2476, June 1997.

[7] Koffi-Kpante, K., Zeitoun, D., and Labracherie, L., "Computation and Experimental Validation of N_2–CH_4–Ar Mixture Flows Behind Normal Shock Wave," *Shock Waves*, Vol. 7, No. 6, 1997, pp. 351–361.

[8] Takashima, N., Hollis, B. R., Zoby, E. V., Sutton, K., Olejniczak, J., Wright, M. J., and Prabhu, D., "Preliminary Aerothermodynamics of

Downloaded by UNIVERSITY OF QUEENSLAND on August 30, 2021 | http://arc.aiaa.org | DOI: 10.2514/1.22095

Titan Aerocapture Aeroshell," AIAA Paper 2003-4952, July 2003.
[9] Olejniczak, J., Wright, M. J., Prabhu, D., Takashima, N., Hollis, B. R., Zoby, E. V., and Sutton, K., "An Analysis of the Radiative Heating Environment for Aerocapture at Titan," AIAA Paper 2003-4953, July 2003.
[10] Olejniczak, J., Prabhu, D., Bose, D., and Wright, M. J., "Aeroheating Analysis for the Afterbody of a Titan Probe," AIAA Paper 04-0486, Jan. 2004.
[11] Wright, M. J., Bose, D., and Olejniczak, J., "The Impact of Flowfield-Radiation Coupling on Aeroheating for Titan Aerocapture," AIAA Paper 04-0484, Jan. 2004.
[12] Park, C., "Assessment of a Two-Temperature Kinetic Model for Dissociating and Weakly Ionizing Nitrogen," *Journal of Thermophysics and Heat Transfer*, Vol. 2, No. 1, 1988, pp. 8–16.
[13] Park, C., *Nonequilibrium Hypersonic Aerothermodynamics*, Wiley, New York, 1990, Chap. 8.
[14] Park, C., Jaffe, R. L., and Partridge, H., "Chemical-Kinetic Parameters of Hyperbolic Earth Entry," *Journal of Thermophysics and Heat Transfer*, Vol. 15, No. 1, 2001, pp. 76–90.
[15] Park, C., Howe, J. T., Jaffe, R. L., and Candler, G. V., "Review of Chemical-Kinetic Problems of Future NASA Missions, 2: Mars Entries," *Journal of Thermophysics and Heat Transfer*, Vol. 8, No. 1, 1994, pp. 9–23.
[16] Park, C., "Review of Chemical-Kinetic Problems of Future NASA Missions, 1: Earth Entries," *Journal of Thermophysics and Heat Transfer*, Vol. 7, No. 3, 1993, pp. 385–398.
[17] Baulch, D. L., Cobos, C. J., Cox, R. A., Prank, P., Hayman, G., Just, Th., Kerr, J. A., Murrels, T., Pilling, M. J., Troe, J., Walker, R. W., and Warnatz, J., "Evaluated Kinetic Data for Combustion Modelling, Supplement I," *Journal of Physical Chemistry Reference Data*, Vol. 26, No. 6, 1994, pp. 847–1033.
[18] Baulch, D. L., Cobos, C. J., Cox, R. A., Esser, C., Prank, P., Just, Th., Kerr, J. A., Pilling, M. J., Troe, J., Walker, R. W., and Warnatz, J., "Evaluated Kinetic Data for Combustion Modelling," *Journal of Physical Chemistry Reference Data*, Vol. 21, No. 3, 1992, pp. 411–429.
[19] Tsang, W., "Chemical Kinetic Data Base for Propellant Combustion 2: Reactions Involving CN, NCO, and HNCO," *Journal of Physical Chemistry Reference Data*, Vol. 21, No. 4, 1992, pp. 753–791.
[20] Tsang, W., and Herron, J. T., "Chemical Kinetic Data Base for Propellant Combustion 1. Reactions Involving NO, NO_2, HNO, HNO_2, HCN and N_2O," *Journal of Physical Chemistry Reference Data*, Vol. 20, No. 4, 1991, pp. 609–663.
[21] Tsang, W., and Hampson, R. F., "Chemical Kinetic Data Base for Combustion Chemistry. Part 1. Methane and Related Compounds," *Journal of Physical Chemistry Reference Data*, Vol. 15, No. 3, 1986, pp. 1087–1279.
[22] NIST Chemical Kinetics Database, Ver. 7.0, 2003.
[23] Dean, A. J., and Hanson, R. K., "CH and C-Atom Time Histories in Dilute Hydrocarbon Pyrolysis: Measurements and Kinetic Calculations," *International Journal of Chemical Kinetics*, Vol. 24, No. 6, 1992, pp. 517–532.
[24] Dean, A. J., Davidson, D. F., and Hanson, R. K., "A Shock Tube Study of Reactions of C Atoms with H_2 and O_2 Using Excimer Photolysis of C_3O_2 and C Atom Atomic Resonance Absorption Spectroscopy," *The Journal of Physical Chemistry*, Vol. 95, No. 1, 1991, pp. 183–191.
[25] Dean, A. J., Hanson, R. K., and Bowman, C. T., "High Temperature Shock Tube Study of Reactions of CH and C-Atoms with N_2," *Twenty-Third Symposium (International) on Combustion*, The Combustion Institute, Pittsburgh, PA, 1990, pp. 259–265.
[26] Davidson, D. F., and Hanson, R. K., "High Temperature Reaction Rate Coefficients Derived from N-Atom ARAS Measurements and Excimer Photolysis of NO," *International Journal of Chemical Kinetics*, Vol. 22, No. 8, 1990, pp. 843–861.
[27] Kruse, T., and Roth, P., "Kinetics of C_2 Reactions During High-Temperature Pyrolysis of Acetylene," *Journal of Physical Chemistry A*, Vol. 101, No. 11, 1997, pp. 2138–2146.
[28] Sommer, T., Kruse, T., and Roth, P., "Perturbation Study on the Reaction of C_2 with N_2 in High-Temperature $C_{60}/Ar + N_2$ Mixtures," *Journal of Physical Chemistry A*, Vol. 101, No. 20, 1997, pp. 3720–3725.
[29] Wooldridge, S. T., Hanson, R. K., and Bowman, C. T., "A Shock Tube Study of Reactions of CN with HCN, OH, and H_2 using CN and OH Laser Absorption," *International Journal of Chemical Kinetics*, Vol. 28, No. 4, 1996, pp. 245–258.
[30] Roose, T. R., Hanson, R. K., Kruger, C. H., "Decomposition of NO in the Presence of NH_3," *Proceedings of the International Symposium on Shock Tubes and Waves*, Vol. 11, University of Washington Press, Seattle, WA, 1978, pp. 245–253.
[31] Mick, H. J., and Roth, P., "High Temperature Thermal Decomposition of CO and CN," *Proceedings of the 18th International Symposium on Shock Waves*, Springer–Verlag, New York, 1991, pp. 805–812.
[32] Gordon, S., and McBride, B. J., "Computer Program for Calculation of Complex Chemical Equilibrium Compositions, and Applications. Analysis Part 1," NASA RP-1311, 1994.
[33] The NASA computer program CEA (Chemical Equilibrium with Applications) website, Oct. 2003 (http://www.grc.nasa.gov/WWW/CEAWeb) [cited October 2003].
[34] The CHEMKIN Collection, Release 3.6.1, Reaction Design, Inc., San Diego, CA.
[35] Markus, M. W., and Roth, P., "On the Reaction of CH with CO Studied in High Temperature $CH_4/Ar + CO$ Mixtures," *International Journal of Chemical Kinetics*, Vol. 24, No. 5, 1992, pp. 433–445.
[36] Kiefer, J. H., and Kumaran, S. S., "Rate of CH_4 Dissociation over 2800–4300 K: The Low-Pressure- Limit Rate Constant," *Journal of Physical Chemistry*, Vol. 97, No. 2, 1993, pp. 414–420.
[37] Lindackers, D., Burmeister, M., and Roth, P., "Perturbation Studies of High Temperature C and CH Reactions with N_2 and NO," *Twenty-Third Symposium (International) on Combustion*, The Combustion Institute, Pittsburgh, PA, 1990, pp. 251–257.
[38] Gökçen, T., "N_2–CH_4–Ar Chemical Kinetic Model for Simulations of Atmospheric Entry to Titan," AIAA Paper 04-2469, June 2004.
[39] Bose, D., Wright, M. J., Bogdanoff, D. W., Raiche, G. A., and Allen, G. A., Jr., "Modeling and Experimental Validation of CN Radiation Behing a Strong Shock Wave," AIAA Paper 05-0768, Jan. 2005.
[40] Bose, D., Wright, M. J., and Gökçen, T., "Uncertainty and Sensitivity Analysis of Thermochemical Modeling for Titan Atmospheric Entry," AIAA Paper 04-2455, June 2004.

Downloaded by UNIVERSITY OF QUEENSLAND on August 30, 2021 | http://arc.aiaa.org | DOI: 10.2514/1.22095